Energy dependence of the $^{119}Sn(p,n)^{119}Sn(IAS)$ reaction*

D. H. Fitzgerald,† G. W. Greenlees, J. S. Lilley, and C. H. Poppe‡
Department of Physics, University of Minnesota, Minneapolis, Minnesota 55455

S. M. Grimes and C. Wong
Lawrence Livermore Laboratory, Livermore, California 94550

(Received 12 August 1977)

Angular distributions for the $^{119}Sn(p,n)^{119}Sb$(isobaric analog state) charge-exchange reaction have been measured at several energies between 16 and 20 MeV using both a neutron-proton coincidence method and a conventional pulsed beam time-of-flight method. The results furnish a value for the relative proton decay width of the analog of the ^{119}Sn ground state: $\Gamma_p/\Gamma = 0.320 \pm 0.015$. The data exhibit the well-known "resonancelike" behavior a few MeV above threshold. Nevertheless, excellent fits to both the magnitude and shape of $\sigma(\theta)$ are obtained with a Lane-model-consistent optical potential, provided that the strength of the neutron absorption potential decreases smoothly in a realistic way with decreasing neutron energy. This modified neutron potential also gives improved fits to low-energy neutron elastic scattering and reaction cross section data.

[NUCLEAR REACTIONS $^{119}Sn(p,n)^{119}Sb$ (IAS), $E_p = 16$, 17, 18, 19, 20 MeV; measured $\sigma(E_p,\theta)$; deduced Γ_p/Γ, isospin form factor, energy dependence of neutron imaginary potential.]

I. INTRODUCTION

For many years, the nucleon-nucleus interaction has been interpreted quite successfully in terms of a first-order picture of a nucleon interacting via an effective force with a distribution of nucleons in a target nucleus. For protons the specifically nuclear part of the interaction can be written in the form[1]: $U_p = -U_0 - \epsilon U_1$, where $\epsilon = (N - Z)/A$. U_0 depends on the average of the p-p and n-p interactions, and the isospin-dependent term U_1 appears directly due to the difference between the n-p and p-p interactions. A simple calculation based on this difference gives $U_1/U_0 \sim 0.5$. An additional term in the proton-nucleus potential of the form $U_C = \alpha Z^2/A^{1/3}$ arises from the Coulomb repulsion and the energy dependence of the nuclear potential. Neglecting dU_1/dE, and taking $dU_0/dE = 0.3$ gives $\alpha \sim 0.4$. For neutrons, the interaction clearly is of the form $U_n = -U_0 + \epsilon U_1$.

Within this framework, a large body of data was analyzed by Becchetti and Greenlees.[2] This included elastic scattering, polarization, and some reaction cross section data for both protons and neutrons at many different energies. An excellent parametrization to the then existing data was obtained. Information also was obtained for U_1 in this global analysis. However, because ϵU_1 is typically only a few percent of U_0, the data analysis was not very sensitive to the isospin term.

The Lane model,[3] which expresses this description of the nuclear interaction in the form

$$U(r) = -U_0(r) + \frac{4}{A}\vec{t}\cdot\vec{T}U_1(r), \tag{1}$$

where A is the mass number of the nucleus and $\vec{t}$ and $\vec{T}$ are the nucleon and nucleus isospin operators, respectively, gives rise to a set of coupled equations. These describe not only elastic nucleon scattering but charge-exchange (quasielastic) scattering as well; in this case the final state of the residual nucleus is the isobaric analog (IAS) of the initial nuclear state. Observation of this phenomenon in the (p,n) reaction was first reported by Anderson and Wong in 1961.[4] Because it is dependent mainly on U_1, the (p,n) charge-exchange reaction has been studied by several groups in recent years[5-12] in order to learn about the strength and form of this term in the nucleon-nucleus potential.

In general, predictions based on global nucleon-nucleus potentials agree remarkably well with the quasielastic data. Improved fits can be obtained; in most cases, these have been achieved by changing the form of the isospin term and readjusting the rest of the optical potential to maintain consistency with the Lane formulation. Recently, a global optical model parametrization based on fits to (p,n) data has been published.[12]

A curious feature of the quasielastic (p,n) data, which is not yet fully understood, is a broad resonancelike maximum in the excitation function of the integrated cross section. This has been noted several times in the literature[6,9-13,14] and occurs essentially in all nuclei a few MeV above threshold.

It is not reproduced by distorted-wave Born approximation (DWBA) or coupled-channels calculations which are based on global optical parameter sets such as those of Becchetti and Greenlees. It has been suggested[10,15,16] that this effect may be due to an energy dependence of the isospin term U_1, an unexplained resonance phenomenon, or to an energy dependence in the optical potential which is not included in current parametrizations.

In general, charge-exchange studies are carried out using pulsed beams and long flight paths in order to obtain adequate neutron energy resolution. However, for nuclei with $A \gtrsim 90$, the excitation energy of the analog state in the final nucleus often is high enough so that it can decay by nucleon emission. Since neutron decay of the IAS to low-lying ($T_<$) states is isospin forbidden, proton ($\tilde{p}$) decay often takes place a significant fraction of the time. This phenomenon was first noted by Yavin *et al.* in 1966.[17] Utilizing this feature we have developed a system similar to that of Woods *et al.*[18] for measuring (p,n) reactions without recourse to beam pulsing techniques. Detecting a proton at the expected energy signals that the $(p,n\tilde{p})$ reaction may have occurred and the neutron time of flight (TOF) is determined relative to it.

The aim of the present work was to investigate the isospin part of the optical potential in the energy region where the anomalous energy behavior has been observed. As is explained below, the n-$\tilde{p}$ coincidence technique is particularly well suited to energies a few MeV above threshold, since the coincidence requirement reduces very considerably the neutron background due to non-charge-exchange processes. In the experiment, the ^{119}Sn(p,n)-^{119}Sb(g.s. IAS) reaction has been studied using both the n-$\tilde{p}$ coincidence and the conventional pulsed-beam methods.

The coincidence measurements were conducted at the University of Minnesota at incident energies of 16, 17, 18, 19, and 20 MeV. The angular distribution of the emitted $\tilde{p}$'s is isotropic, and so these measurements yield the quantity

$$\sigma_{p,n}(E_p, \theta_n)\Gamma_{\tilde{p}}/\Gamma, \tag{2}$$

where $\sigma_{p,n}(E_p, \theta_n)$ is the (p,n) cross section, at bombarding energy E_p, for the analog transition, measured at an angle θ_n with respect to the incident beam direction. $\Gamma_{\tilde{p}}/\Gamma$ is the relative probability that the IAS will decay by proton emission; i.e., $\Gamma_{\tilde{p}}$ is the partial decay width for protons, and Γ is the total decay width of the IAS.

Measurements using the conventional method were carried out at the Lawrence Livermore Laboratory (LLL) at incident energies of 17, 18, 19, and 20 MeV. Systematic errors between the two data sets were minimized and excellent agreement of the angular distributions was obtained at all four energies. This enabled us to determine $\Gamma_{\tilde{p}}/\Gamma$ by a scale comparison of the two sets of angular distributions.

Of additional interest was the observation, in the concidence experiment, of the population and decay of the analogs (in ^{119}Sb) of excited states of ^{119}Sn.[19] Because these phenomena lie outside the scope of the Lane model and depend on the nuclear spectroscopy of the nuclei being studied, details of this work are reported in a separate paper.

II. EXPERIMENT

A. *n-p* coincidence measurements (Minnesota)

Protons from the University of Minnesota tandem accelerator were incident on a 2 mg/cm^2 target of enriched (89.8%) ^{119}Sn.[20] Neutrons were detected in an array of five cylindrical, 5.80 cm $\times$ 5.80 cm NE213 scintillators.[21] The target-to-scintillator distance was typically 40 cm. Almost all γ-ray events were eliminated using conventional pulse shape discrimination techniques (PSD). A linear signal threshold was set at the pulse height corresponding to the midpoint of the Compton edge from a ^{22}Na source. This corresponds to a minimum neutron detection energy of 1.6 MeV.[22] Charged particles were recorded in two Si surface barrier detector telescopes each consisting of an E detector, capable of stopping 10 MeV protons, followed by a "VETO" detector, used to eliminate signals from passing particles, notably those which had been elastically scattered by the target. The E-VETO stacks were mounted in the vertical plane ($\phi = \pm 90°$) at an angle of 135° to the incident beam direction. The backward angle was chosen to minimize the elastic counting rate, which is the main factor limiting the data collection rate. The proton detector solid angles were maximized by using large circular apertures (7.6 mm diam) close (2.8 cm) to the target. At this distance, thin (2.2 mg/cm^2) nickel foils were needed in front of the detectors to protect them from a large flux of electrons from the target.

The neutron TOF was determined as the time difference between the neutron timing signal (STOP) and a timing signal (START) inductively derived from the output of the E detector. After being processed by an analog-to-digital converter (ADC), coincident TOF-$E_{\tilde{p}}$ signal pairs were routed into one of the five two-dimensional computer arrays, corresponding to the proper neutron detector. Soft-ware windows were set in the $\tilde{p}$ spectrum in the energy region expected for the 7.21 MeV ground-state (g.s.) analog $\tilde{p}$ decay and gated TOF spectra were accumulated for each neutron detector.

In addition, the TOF-$E_{\tilde{p}}$ coincidences were dumped on magnetic tape to be replayed later in off-line analyses with new gating criteria.

B. Pulsed-beam neutron measurements (Livermore)

Neutrons from the $^{119}Sn(p,n)$ reaction were detected at angles between 13.5° and 159° in an array of sixteen NE213 scintillators. The target-to-scintillator distance was 10.8 m. Conventional PSD again was used to reduce γ-ray background, and the linear pulse height threshold was 1.6 MeV, identical to that in the coincidence experiment. Two targets were used in the measurements: the target used in the coincidence measurements described above, and a 5.0 mg/cm^2 ^{119}Sn target which also was enriched to 89.8%. The relative target thicknesses were determined to within ±3% by means of overlap runs. The relative neutron detector efficiencies for the "Minn" and "LLL" systems were determined to within ±1.3% over the energy range of the experiment by directly comparing the observed yields from the $^2H(d,n)^3He$ reaction at a number of energies. The absolute neutron detection efficiency of the LLL detectors had been previously determined[11] to within ±7%.

III. RESULTS

A. Coincidence measurements

A $(p,n\tilde{p})$ excitation function was taken with the neutron detectors at 36°, 48°, 60°, 72°, and 84°, for incident proton energies ranging from 16 to 20 MeV in 1.0 MeV steps. For two energies (17 and 19 MeV) neutron angular distributions, in 6° steps, were obtained over a wider angular range. At each angle, between 300 and 1800 counts (depending on the counting rate) were obtained in the g.s. analog neutron peak, resulting in statistical uncertainties of 3–10% after background subtraction.

Figure 1(a) shows a typical TOF spectrum, gated by protons with energies near 7.21 MeV, the $\tilde{p}$ energy for g.s. analog decay to the g.s. of ^{118}Sn. In this case, the incident energy was 17 MeV and the neutron detector angle was 48°. The peak labeled γ is due to γ ray events, which were deliberately allowed to "leak" through the PSD neutron window. The strong peak at 3.2 MeV labeled n is due to exciting the g.s. analog and corresponds to neutrons with energies near 3.2 MeV. Typically, the TOF time resolution was 1.7 nsec [full width at half maximum (FWHM)], which gives a neutron peak width of about 600 keV for 3.2 MeV neutrons. The 1.6 MeV neutron energy threshold also is indicated in the figure.

In order to simplify background subtraction, an

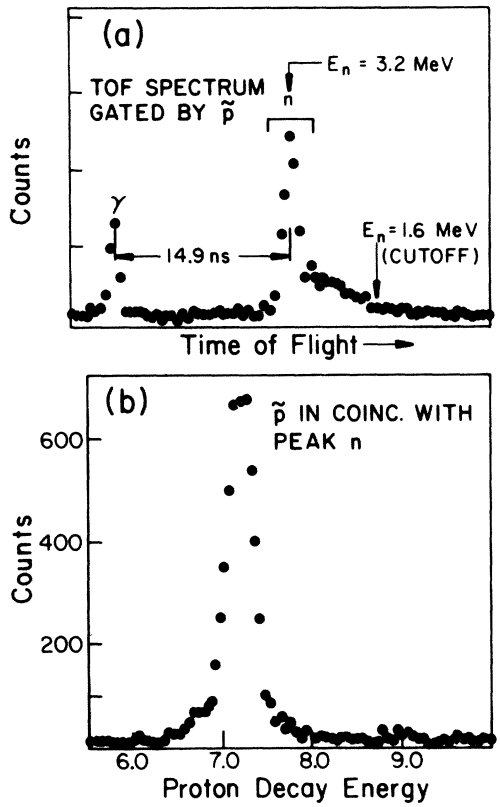

FIG. 1. (a) Neutron time-of-flight spectrum for the reaction $^{119}Sn(p,n\tilde{p})^{118}Sn$ taken at 48° and incident energy of 17 MeV, gated by protons with energies near 7.21 MeV. A γ-ray peak and a 3.2 MeV neutron peak due to quasielastic scattering are shown as well as the detection threshold corresponding to 1.6 MeV neutrons. (b) Decay-proton spectrum in coincidence with 3.2 MeV neutrons, after background subtraction.

off-line analysis of these data was conducted by replaying the raw data tapes with the coincidence requirements reversed. Proton energy spectra, gated by the 3.2 MeV neutron group were extracted. The accidental background in the proton spectra was obtained in a separate pass through the raw data, by gating on an appropriate region of the TOF spectrum. These background spectra were subtracted from the neutron-gated proton spectra. Figure 1(b) shows such a spectrum after accidental background subtraction. The net yield for the g.s. analog reaction was obtained from the number of counts in the 7.2 MeV proton peak above a linear background. This was compared, in each case, with the yield obtained from the corresponding proton-gated TOF spectrum, and uniformly excellent agreement was obtained. For the angular distributions at 17 and 19 MeV, overlap runs were performed using two or more different neutron detectors at nearly every angle. Reproduci-

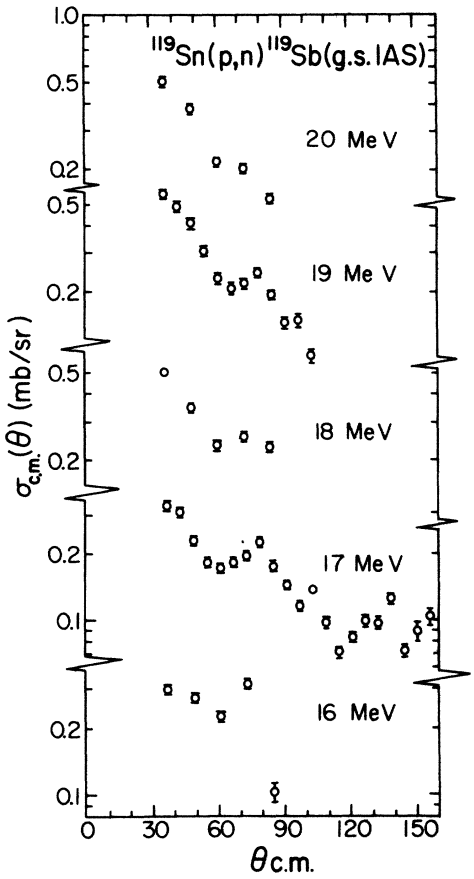

FIG. 2. Angular distributions taken at $E_p = 16$, 17, 18, 19, and 20 MeV using the n-p coincidence technique of the ^{119}Sn$(p,n\tilde{p})^{118}$Sn reaction.

bility well within statistical uncertainty was obtained at each angle for the g.s. analog yields.

Based on these yields, absolute differential cross sections were obtained using a calculation which included target thickness, integrated beam current, neutron detection efficiency, and finite solid angle effects in both the $\tilde{p}$ and neutron detectors. The main contributions to systematic uncertainties in this calculation came from: the LLL measurement of the neutron detection efficiency (±7%); normalization of Minn to LLL detectors (±1.3%); estimated attenuation in the scattering chamber wall (±2%); and the measurement of target thickness (±2%). The resulting overall scale uncertainty for the g.s. analog cross section is ±8%. Figure 2 shows the angular distributions for the g.s. $(p,n\tilde{p})$ reaction at 16, 17, 18, 19, and 20 MeV.

B. Pulsed-beam measurements

Figure 3 shows a portion of a typical TOF spectrum. In contrast to the proton-gated TOF spectrum above, the IAS neutron spectrum is superimposed on a substantial background due to (p,n) reactions proceeding to $T_<$ states in ^{119}Sb. The peak-to-background ratio for the g.s. analog peak was typically 2.5 to 1. In this case, the TOF time resolution was 1.5 nsec or 120 keV (FWHM).

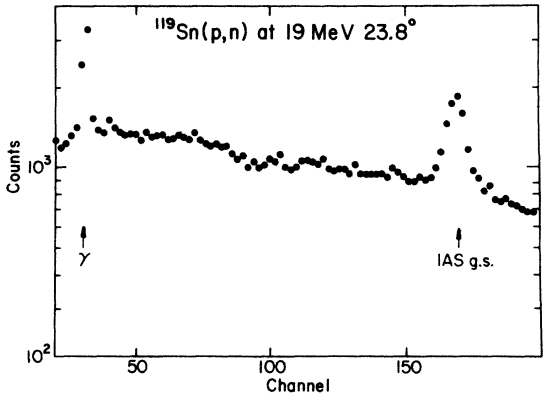

FIG. 3. Portion of a conventional pulsed-beam time-of-flight spectrum taken at Lawrence Livermore Laboratory of the ^{119}Sn$(p,n)^{119}$Sb reaction at 23.8° and 19 MeV bombarding energy, showing a γ peak and the ground-state analog peak.

The differential cross section was calculated from the net counts above background for the g.s. analog peak. The resulting angular distributions are shown in Fig. 4 (solid circles). The overall scale uncertainty for these measurements is ±8%.

C. Integrated cross sections and relative proton decay widths

From expression (2), a comparison of the n-$\tilde{p}$ coincidence and pulsed-beam (p,n) angular distributions will yield the relative proton decay width, $\Gamma_{\tilde{p}}/\Gamma$. In Fig. 4 the angular distributions for the $(p,n\tilde{p})$ g.s. analog reaction (open circles) have been scaled at 17, 18, 19, and 20 MeV to agree in magnitude with the (p,n) cross sections. Excellent agreement in angular distribution shape is seen between the two data sets. $\Gamma_{\tilde{p}}/\Gamma$ was obtained at each energy as the scale factor between the data sets, and the values are reassuringly energy-independent (see Table I). This direct comparison supports the validity of the n-$\tilde{p}$ coincidence method for studying the angular and energy dependence of the (p,n) analog reaction. Furthermore, the comparison accurately determines $\Gamma_{\tilde{p}}/\Gamma$ since the effects of neutron detector efficiency and target thickness cancel to first order and the corresponding systematic uncertainties are negligible. Thus the errors shown for $\Gamma_{\tilde{p}}/\Gamma$ in Table I represent only statistical uncertainties between the two data sets. The error weighted average of these values was adopted as the g.s. analog relative pro-

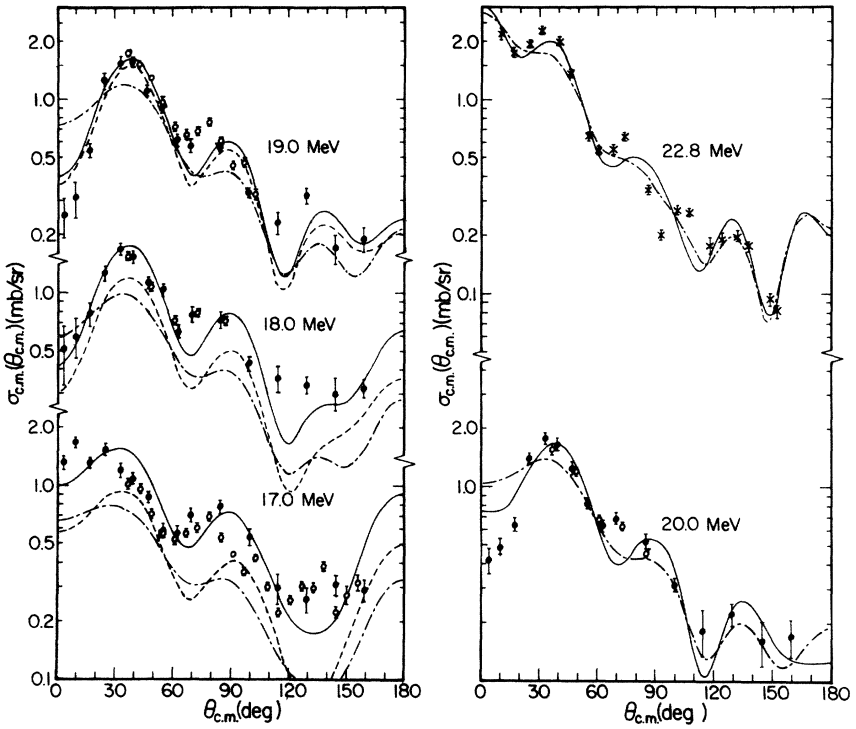

FIG. 4. Differential cross sections for the $^{119}Sn(p,n)^{119}Sb$(g.s. IAS) reaction taken at 17, 18, 19, 20, and 22.8 MeV. The open circles are the $(p,n\tilde{p})$ data of Fig. 2 scaled as described in the text to the (p,n) data (closed circles) taken at Livermore. The 22.8 MeV data (crosses) are those of Ref. 5. The curves are DWBA calculations using different parameter sets: dot-dashed curve, DWBA I; dashed-curve, DWBA II; and solid curve, DWBA III.

ton decay width:

$$\Gamma_{\tilde{p}}/\Gamma = 0.320 \pm 0.015 .$$

The integrated cross section $\sigma_{int}(p,n)$ at each bombarding energy was obtained from a Legendre polynomial fit to the angular distribution. These values also are shown in Table I, along with the values of $\sigma_{int}(p,n)\Gamma_{\tilde{p}}/\Gamma$ inferred from the scale comparison. At 16 MeV, $\sigma_{int}(p,n)\Gamma_{\tilde{p}}/\Gamma$ was estimated by scaling the n-$\tilde{p}$ coincidence data to the 17 MeV pulsed-beam data. From Fig. 4, the angular behavior of the data between 36° and 84° varies quite slowly with energy, so this is probably a reasonable procedure.

The present result for $\Gamma_{\tilde{p}}/\Gamma$ may be compared with the ratio Γ_p/Γ measured for the g.s. analog in proton elastic resonance scattering. In general, these two values may not be compared directly because the $\tilde{p}$ measurement includes both the intrinsic proton width of the analog state Γ_p and the "spreading" width W due to Coulomb mixing of the analog state with nearby $T_<$ states (e.g., see Ref. 23). If the $T_<$ states themselves have large proton decay widths, then $\Gamma_{\tilde{p}} > \Gamma_p$. For ^{119}Sn, however, the $T_<$ states may neutron decay and this mode should dominate strongly over proton emission, which is inhibited by the Coulomb barrier. In the present case, therefore, the effect of the spreading width on $\Gamma_{\tilde{p}}$ is small and to a good approximation, $\Gamma_{\tilde{p}} = \Gamma_p$. The result of the present experiment is in excellent agreement with $\Gamma_p/\Gamma = 0.34$, measured by Richard *et al.*[24] Both these results are somewhat lower than the value, 0.38 ±0.05, obtained in single $\tilde{p}$ measurements by Miller and Garvey.[13] This discrepancy is discussed in a separate paper which deals with the observation of analogs of excited states in ^{119}Sn.

IV. ANALYSIS AND DISCUSSION

A. Theory

The (p,n) charge-exchange reaction from the g.s. of the (N,Z) nucleus to its analog in the $(N-1, Z+1)$ nucleus is described by one of the off-diagonal matrix elements of Eq. (1):

$$U_{pn}(r) = 2(N-Z)^{1/2}U_1(r)/A \qquad (3)$$

In the usual direct reaction theory, U_{pn} is the charge-exchange interaction potential used to calculate the transition amplitude in the distorted-wave Born approximation (DWBA) (see, for example, Ref. 1):

TABLE I. Integrated cross sections and relative proton decay widths.

Measurement Lab energy (MeV)	LLL (p,n) $\sigma_{\text{int}}(p,n)$ (mb)	Minn $(p,n\tilde{p})$ $\Gamma_{\tilde{p}}/\Gamma$	Minn $(p,n\tilde{p})$ $\sigma_{\text{int}}(p,n)\Gamma_{\tilde{p}}/\Gamma$ (mb)
16	•••	•••	~2.2 (±0.4)
17	7.88±0.25	0.305±0.02	2.40±0.17
18	8.26±0.26	0.32 ±0.03	2.64±0.25
19	7.03±0.18	0.335±0.02	2.35±0.15
20	6.79±0.21	0.31 ±0.03	2.10±0.22

$$T_{pn}^{\text{DWBA}}(\theta)=\frac{2(N-Z)^{1/2}}{A}\times\int\chi_{nA0}^{(-)*}(\vec{k}_n,\vec{r})U_1(r)\chi_{pc0}^{(+)}(\vec{k}_p,\vec{r})d^3r\,.$$

The distorted waves $\chi_{nA0}^{(-)}$ and $\chi_{pc0}^{(+)}$ are generated using optical potentials $\hat{U}_n$ and $\hat{U}_p$, which fit observed neutron and proton elastic scattering, respectively. It must be noted that neutron scattering from the analog state cannot be observed when it is an excited state. However, the optical potentials vary slowly with energy and mass number. Therefore, it is a reasonable approximation to use potential parameters corresponding to neutron scattering from the parent of the analog state (the g.s. of ^{119}Sn in the present case) evaluated at the appropriate outgoing neutron energy.

The proton and neutron nuclear optical potentials used were of the form

$$U(r)=-Vf(r_R,a_R)-iW^vf(r_I,a_I)+iW^s4a_I\frac{df}{dr}(r_I,a_I)+V_{so}\lambda_\pi^2\frac{(\vec{l}\cdot\vec{\sigma})}{r}\frac{df}{dr}(r_{so},a_{so})\,,\qquad(4)$$

where the radial shapes all have a Woods-Saxon form:

$$f(r_i,a_i)=\{1+\exp[(r-r_iA^{1/3})/a_i]\}^{-1}\,.$$

As pointed out by Satchler,[1] it is reasonable to expect U_1 to be complex. For the optical potentials used in the present analysis, the volume absorption strength W^v is small compared to the surface strength W^s in the energy region considered. In fact, W^v often is taken to be zero for neutrons with up to approximately 7 MeV, which for ^{119}Sn$(p,n)^{119}$Sb(g.s. IA) corresponds to 20 MeV incident protons. Initially, therefore W_1 the imaginary part of U_1, was given the same surface form as W^s.

B. DWBA analysis: Initial parametrization

As a starting point in the analysis, the Becchetti-Greenlees[2] (BG) "best fit" proton and neutron optical potential parameters were chosen. These parameters are listed as Set A in Table II. The proton and neutron energies are related by $E_n=E_p-\Delta_C$, where Δ_C is the Coulomb displacement energy for the analog transition. The ϵ terms are the symmetry energy terms in the diagonal matrix elements of Eq. (1).

The interaction potential had the form:

$$U_{pn}(r)=V_{pn}(r)+iW_{pn}(r)=2\frac{(N-Z)^{1/2}}{A}[V_1f(r_{1R},a_{1R})+4iW_1^sa_{1I}\times\frac{df}{dr}(r_{1I},a_{1I})]\,,\qquad(5)$$

where

$$V_1=24.0\text{ MeV},\quad r_{1R}=1.17,\quad a_{1R}=0.75\,,$$

and

$$W_1^s=12.0\text{ MeV},\quad r_{1I}=1.29,$$

$$a_{1I}=0.5[1.09+0.7(N-Z)/A]\qquad(6)$$

were determined from the $(N-Z)/A$ dependent terms in the Set A parameters. The imaginary radius and diffuseness parameters were taken to be the average of the appropriate proton and neutron parameters.

The DWBA predictions using Set A and Eqs. (5) and (6) will be referred to as DWBA I. The use of these parameters has produced a reasonable representation of the average behavior of charge-exchange data for a wide range of targets and bombarding energies (e.g., see Refs. 5 and 8). In this respect, the parametrization forms an excellent starting point for the investigation which follows in the next section.

The DWBA I curves (dot-dashed) are compared in Fig. 4 with the Minn $(p,n\tilde{p})$ and the LLL (p,n) results at 17, 18, 19, and 20 MeV, and results at 22.8 MeV from Ref. 5. The computer code DWUCK[25] was used to perform the calculations. As can be seen, the observed behavior with angle is

TABLE II. Optical model parameters. Parameters from Ref. 2. $\gamma = Z/A^{1/3}$, $\epsilon = (N-Z)/A$, W^v and $W^s \geq 0$ always. All potentials are in MeV and all distances are in fm.

	Set A	Set B
V_p	$54.0 - 0.32E_p + 0.4\gamma + 24\epsilon$	$55.2 - 0.32E_p + 0.27\gamma + 24\epsilon$
W_p^v	$0.22E_p - 2.7$	$0.22E_p - 0.18\gamma - 1.4$
W_p^s	$11.8 - 0.25E_p + 12\epsilon$	$10.2 - 0.25E_p + 0.21\gamma + 12\epsilon$
V_n	$56.3 - 0.32E_n - 24\epsilon$	$55.2 - 0.32E_n - 24\epsilon$
W_n^v	$0.22E_n - 1.6$	$0.22E_n - 1.4$
W_n^s	$13.0 - 0.25E_n - 12\epsilon$	$12.0 - 0.25E_n - 12\epsilon$
	$r_{Rp} = r_{Rn} = 1.17$, $a_{Rp} = a_{Rn} = 0.75$, $V_{so} = 6.2$, $r_{so} = 1.01$, $a_{so} = 0.75$,	
	$r_{Ip} = 1.32$, $a_{Ip} = 0.51 + 0.7\epsilon$, $r_{In} = 1.26$, $a_{In} = 0.58$	

reproduced surprisingly well, considering the approximations employed in extracting U_{pn} as a small difference between $\hat{U}_n$ and $\hat{U}_p$.

Nevertheless, significant departures from the DWBA predictions are present. In particular, the overall magnitude of the cross sections is not well reproduced for the lower energies. The discrepancy is most noticeable at 17 MeV, where the DWBA cross section is less than 60% of that seen experimentally. The magnitude of the discrepancy decreases with increasing bombarding energy, and excellent agreement is obtained with the cross section magnitude at 22.8 MeV. Similar discrepancies have been noticed for the (p,n) analog reaction on all target nuclei for which measurements have been made near the reaction threshold (e.g., see Refs. 10 and 11).

The DWBA I curves also fail to reproduce the observed behavior at forward angles, over the energy range considered. In particular, the forward-angle dip in the data at 18, 19, and 20 MeV is not seen in the DWBA curves. This forward-angle behavior is discussed in the next section in terms of the form used for the interaction potential U_{pn}.

C. DWBA analysis: Consistency with the Lane model

If Coulomb effects are neglected, then in the Lane model, U_{pn}, U_n, and U_p must be related in the following manner:

$$U_{pn} = (N-Z)^{-1/2}(U_n - U_p)\,. \tag{7}$$

In spite of the apparent simplicity of this relation, care must be exercised in its application if U_n and U_p are approximated by optical potentials $\hat{U}_n$ and $\hat{U}_p$ derived from elastic scattering data. All components of $(\hat{U}_n - \hat{U}_p)$ should exhibit an $(N-Z)$ dependence, and, because the incident proton energy differs (by Δ_C) from the outgoing neutron energy, this condition can be satisfied only if there are Coulomb terms in the proton potential which correct for the energy dependence of all components of the potential strengths in such a way that the isoscalar terms in both channels are the same.

Most optical model sets have a Coulomb term in the real central strength only which does not compensate completely for the neutron-proton energy difference. A potential set which more closely satisfies the requirement for all terms in the potential is the set of Ref. 2 labeled $V_C = 0.84$ for protons, and "common" for neutrons. These are listed in Table II as Set B.

Since the Coulomb energy of the proton averaged over the target nucleus is approximately equal to Δ_C, it is reasonable to obtain the (p,n) form factor from a Lane-consistent optical potential evaluated at an energy which is the average of the Coulomb-corrected proton energy and the neutron energy. This was done in a recent global analysis[12] of (p,n) charge-exchange data, based on the optical parameters of Set B. However, in the work of Ref. 12, the neutron and proton potentials were constrained to have the same geometry. In the present analysis, consideration of the shape of the neutron and proton potentials led to another method of approximating this form factor as explained below.

If Eq. (7) is used to obtain U_{pn} from the Set B optical potentials, the choice of the geometry parameters for W_{pn}^s, the imaginary part of U_{pn}, requires some care because, in general, the shapes of the isovector imaginary parts of $\hat{U}_n$ and $\hat{U}_p$ are different. The Coulomb barrier causes the wave functions of the bound protons to fall off more rapidly than the neutron wave functions in the nuclear surface. This qualitative expectation is supported by an analysis[26] of scattering data for heavy nuclei which shows the neutron distribution to have a rms radius slightly larger than that of the proton dis-

tribution. In addition, a recent analysis[27] of (p,n) charge-exchange data for even Sn isotopes indicates that the ratio of the neutron to proton rms radii increases with increasing neutron excess. This should cause W_p, the absorptive potential for incident protons, to be displaced to slightly larger radii than that for neutrons W_n, because the p-n interaction is about 2.5 times as strong as the n-n or the p-p interaction.

Often, as in the preceding section, analyses of the (p,n) analog reaction employ an average of the parameters used in W_p and W_n (e.g., Refs. 6 and 8). However, if the neutron excess is concentrated near the nuclear surface, it is more likely that charge exchange will occur in this region than in the interior. Then the use of average values for the radius and diffuseness of W_{pn} may overlook an important facet of the (p,n) analog reaction.

Accordingly, a new set of predictions, which will be referred to as DWBA II, were generated in order to investigate the effect of changing the shape of W_{pn}. The optical potentials were those of Set B (Table II), V_{pn} was left unchanged, and W_{pn} was evaluated for each value of the nuclear radius using the relation

$$W_{pn} = (N-Z)^{1/2}[W_n^s(E_n, r_{In}, a_{In}) - W_p^s(E_p, r_{Ip}, a_{Ip})] . \quad (8)$$

This procedure resulted in form factors for W_{pn} which had different shapes and peaked about 0.5 fm further out in the nuclear surface compared with those of DWBA I.

The DWBA angular distributions using these potentials are shown as the dashed curves in Fig. 4. Compared to DWBA I (dot-dashed curves), DWBA II gives considerably improved agreement with the observed angular distributions, especially at angles forward of 60°, and demonstrates the sensitivity of the calculations to the geometry chosen for the interaction potential. (DWBA predictions calculated with the Set B optical potentials but the same interaction potential as DWBA I have the same shape as the DWBA I curves.)

Theoretical curves also were generated using the parameter set of Ref. 12. These parameters differ from Set B chiefly in that (a) W_1^s is energy-dependent, (b) $W_1^s/V_1 \simeq 1$, and (c) the neutron and interaction form factor absorption geometry equals that for the protons: $r_I = 1.32, a_I = 0.51 + 0.7[(N - Z)/A]$. This last change means that, just as for Set B, W_{pn} extends to larger nuclear radii than if an average of neutron and proton geometries is used. In fact, the W_{pn} centroids for the Ref. 12 and DWBA II predictions agree to within a few percent, and the quality of fit to the data is essentially the same as that of DWBA II. These results lend support to the argument that the (p,n) analog transition at forward angles is sensitive to the location of the neutron excess, in agreement with the results of Batty, Friedman, and Greenlees.[28]

D. Energy dependence

The agreement with the cross section magnitudes is improved only slightly with this new parametrization of $W_1(r)$. A more complete view of this magnitude discrepancy appears in Fig. 5, which shows the energy behavior of the integrated cross section obtained from the data and DWBA calculations (Sets I and II) of Fig. 4. The discrepancy near the reaction threshold is perhaps not surprising in view of the ambiguities in the energy dependence of U_{pn}. Nevertheless, attempts to fit a similar energy behavior for other target nuclei, using channel coupling[29] or an *ad hoc* energy dependence in the interaction potential[14] have been unsatisfactory.

However, Garvey and Miller[16] have reported that the (p,n) reaction strength for ^{91}Zr is extremely sensitive to variations in the neutron imaginary potential. More recently, Kunz *et al.*[15] have shown that using neutron parameters derived from low-energy neutron scattering produces satisfactory results near the (p,n) reaction threshold in the case of ^{208}Pb.

Accordingly, an investigation was made to see what changes occurred in the DWBA II results when the strength W_n^s was varied in Set B and Eq. (8). That is, a DWBA III parameter set was defined with the neutron and proton optical parameters of Set B, except that W_n^s was replaced by

$$W_n^s = F[12.0 - 0.25E_n - 12(N-Z)/A] , \quad (9)$$

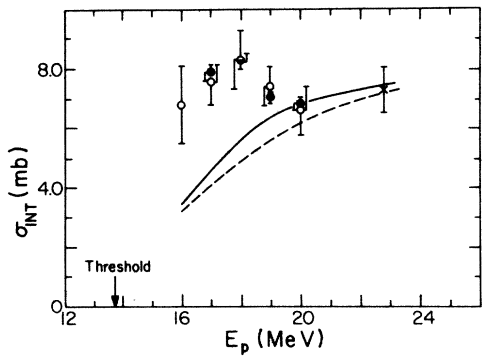

FIG. 5. Integrated quasielastic ^{119}Sn$(p,n)^{119}$Sb reaction plotted as a function of incident (lab) proton energy. Symbol identification is the same as that for Fig. 4. The reaction threshold is shown at $E_p = 13.8$ MeV. Theoretical curves shown were calculated using parameters of DWBA I (dashed) and DWBA II (solid).

where F is a variable parameter. This expression for W_n^s also was used in the determination of the imaginary part of the interaction potential from Eq. (8). The real part was unchanged from DWBA II. A grid search (step length = 0.005) was used to determine at each energy the value of F for which the calculated integrated (p,n) cross section equaled the measured value. Figure 6(a) shows the values of F determined in this fashion, plotted against energy. The error bars for F reflect the uncertainty in the measured cross section value at each energy. As can be seen, F falls off smoothly as E_n decreases below 6.2 MeV [corresponding to 20 MeV incoming protons in the (p,n) reaction].

The energy dependence of the absorptive potential, corresponding to the F values of Fig. 6(a) is shown in Fig. 6(b). Here the volume integral of $W_n(r)$ is plotted against c.m. neutron energy. The neutron separation energy is indicated by the arrow and the point near $E_n = 0$ was determined from an overall optical model fit to the s-wave neutron strength function for nuclei.[30] It should be noted that the neutron absorption potential in the BG global set always increases as E_n decreases [solid curve in Fig. 6(b)]. However, $W_n(r)$, which is zero for neutrons near the Fermi energy, initially should increase with increasing neutron energy as new reaction channels open up, and a low-energy dependence such as the one shown as the dashed curve in Fig. 6(b) is to be expected.

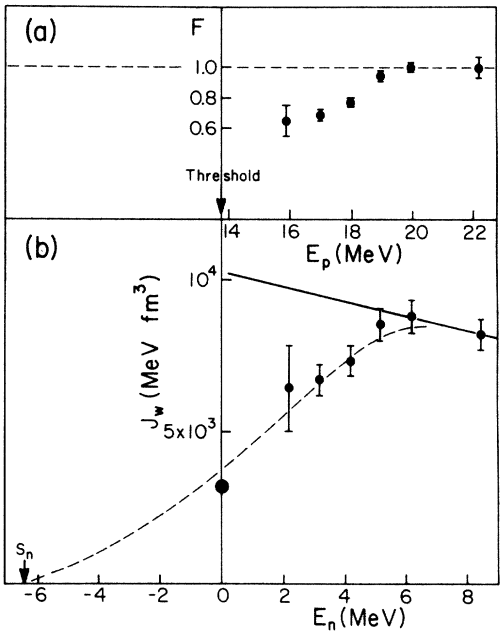

FIG. 6. (a). Values of the neutron imaginary potential scaling factor F [see Eq. (9)] required to achieve fits to the data of Fig. 5, plotted versus incident (lab) proton energy. (b). Volume integral of the neutron imaginary potential versus c.m. neutron energy. The points for $E_N > 2$ MeV are values used in the DWBA III fits to the present data. The point near $E_n = 0$ was determined from an optical model fit to the s-wave neutron strength function for nuclei (Ref. 30), and the neutron separation energy is indicated by the arrow. The solid curve is given by the parameters of Set B of Table II; the dashed curve is to guide the eye.

DWBA angular distributions obtained using parameter Set III are compared with data in Fig. 4 (solid curves). Significant overall improvement in agreement with the data has been achieved, over that found using the BG "best" fit parameters. The stepwise improvement of the agreement may be appreciated by comparing the "best" fit DWBA I curves and the intermediate (DWBA II) results with the DWBA III curves. (Note that the results for DWBA II and III at $E_p = 20$ and 22.8 MeV are identical, because $F = 1$ for these energies.) The improvement can be attributed to two factors. The neutron and proton absorption terms were parametrized separately in W_{pn}^s, moving it out to large nuclear radii. Secondly, the absorption term in the neutron potential was given a more realistic behavior at low energies. We have recently duplicated these results in a coupled-channels calculation in which the overall potential well depths were equal to those of DWBA III, but in which the ratio U_1/U_0 was slightly modified so that strict consistency with the Lane model was maintained for imaginary parts as well as for the real parts of the potentials.

As a test of this "more realistic" neutron potential, predictions using the DWBA III parameters have been compared with available neutron elastic scattering,[31] total reaction,[32] and nonelastic[33] cross sections for natural Sn in the energy range for neutrons in the present analysis (2 to 9 MeV), and with elastic scattering on Sb at 8.05 MeV.[34] The values of F, and therefore W_n^s, at neutron energies other than those of the (p,n) data were obtained from a smooth curve drawn through the points of Fig. 6(a). The data and DWBA III predictions (solid curves) are presented in Fig. 7. For the total reaction and nonelastic cross sections, the results obtained using the Becchetti-Greenlees "common" neutron parameters are shown as dashed curves. The calculated elastic scattering and nonelastic cross sections include the results of a rather extensive Hauser-Feshbach compound elastic (CE) cross section calculation. Details of the calculation are described in the following paragraph. As can be seen in Fig. 7, predictions of neutron data, particularly total cross sections, using DWBA III neutron parameters show excellent agreement with the data and represent a con-

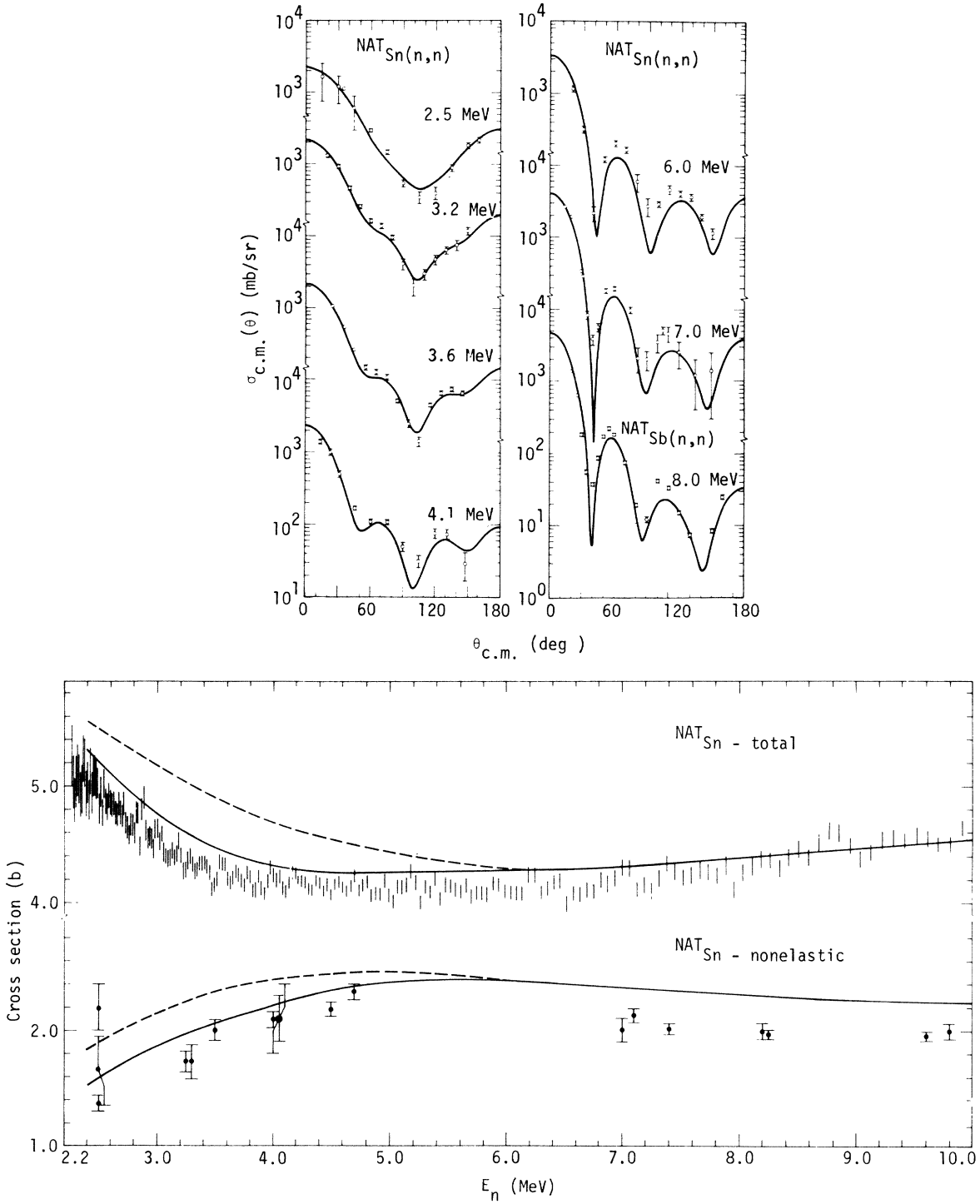

FIG. 7. (a). Differential cross section for neutron elastic scattering at various bombarding energies. The data are for natural Sn (Ref. 31) with the exception of the 8.0 MeV cross section which is for natural Sb (Ref. 34). The solid curves are optical model predictions using DWBA III neutron potential parameters and including the effects of compound elastic scattering. (b) Neutron total and nonelastic cross sections. The total cross section data are those of Ref. 32; the nonelastic data are from Ref. 33. In both cases, the dashed curves are the results of an optical model prediction using the Becchetti-Greenlees "common" neutron parameters (Set B of Table II). The solid curves are similar calculations using the DWBA III neutron parameters. For both sets of parameters a correction for compound elastic scattering was applied to the calculated nonelastic cross section.

siderable improvement over results obtained using BG "common" parameters. The agreement with the DWBA III parameters seems best at energies between 2 and 6 MeV. Above 6 MeV, the agreement with the total cross section is still excellent, but the elastic scattering predictions fall somewhat below the data, while the nonelastic scattering predictions are 10% high. This suggests that the energy behavior of W_n for $E_n > 6$ MeV is still not quite correctly represented by the parameters of DWBA III. Nevertheless, the overall agreement with the neutron data is impressive and is comparable in most cases to that obtained by fitting the data.

The Hauser-Feshbach CE corrections were inferred from a statistical calculation of the (n,n'), (n,p), and (n,α) cross sections for energies up to 9 MeV. They were found to be negligible for energies above 5–6 MeV. The cross sections were represented by a Legendre polynomial expansion up to order 4. The optical potentials used in the calculation were the Becchetti-Greenlees "best" fit parameters for $n+^{119}Sn$ and $p+^{119}In$, and the Huizenga-Igo[35] parameters for $\alpha+^{116}Cd$. The choice of parameters and isotopes is expected to have little effect on the values of the transmission coefficients calculated for the corrections. However, for spin coupling, level densities in the residual nuclei and excitation energies, the structure of nuclear isotopes considered is important, so natural Sn was represented as being composed of 20.2% ^{116}Sn, 33.8% ^{118}Sn, and 46.0% ^{120}Sn, which are its major constituents. The various angular momentum sums were carried out for up to the highest spins expected in the compound and residual nuclei consistent with known level schemes, and the distribution of spins in the statistical model. Above the highest known levels, the level density was calculated from a constant temperature model for excitation energies below 5 MeV and from a Fermi gas model above 5 MeV. Pairing energies, nuclear temperatures, and Fermi gas parameters were taken or interpolated from the compilation of Gilbert and Cameron.[36] Finally, a correction was made for width fluctuation correlations, following Moldauer.[37]

V. SUMMARY

The neutron-proton coincidence technique has been used successfully to study the $^{119}Sn(p,n)^{119}Sb(IAS)$ reaction near threshold. The accuracy of the data is comparable with or better than that of data taken using the conventional pulsed-beam method, and the comparison of results of both methods gives directly the relative proton decay width of the ground-state analog: $\Gamma_p/\Gamma = 0.320 \pm 0.015$.

The $^{119}Sn(p,n)^{119}Sb$ reaction can be accounted for entirely in terms of a generalized optical model, not only at high energies, where global optical potentials give a satisfactory prediction, but also at energies near threshold provided the neutron imaginary potential is modified. Excellent fits are obtained to quite detailed angular distributions covering this "anomalous" region with (i) the isospin form factor calculated from the difference of the neutron and proton form factors, which, in general have different imaginary geometries, and (ii) the strength of the Becchetti-Greenlees neutron imaginary potential multiplied by a factor which decreases smoothly from unity at about 20 MeV (incoming proton energy) to a value of about 0.6 at 16 MeV. Since the outgoing neutron energy changes by about a factor of 3 over the energy range studied and the imaginary potential is expected to decrease at low energies, this behavior is thought to be physically reasonable. The modified potential gives improved fits to neutron elastic scattering and total reaction cross section data; the change in the (p,n) cross section is dramatic and amounts to nearly a factor of 2 in an extreme case.

Although it cannot be said that this is a complete explanation of the near threshold maximum in the (p,n) cross section, it is confirmed that the (p,n) reaction is most sensitive to the neutron optical potential and particularly to the imaginary term. Any attempt to understand the near threshold behavior of the (p,n) reaction must take this sensitivity into account.

---

*Supported in part by the U. S. Energy Research and Development Administration.

†Current address: Crocker Nuclear Laboratory and Department of Physics, University of California, Davis, California 95616.

‡On leave of absence at Lawrence Livermore Laboratory, Livermore, California 94550.

[1]G. R. Satchler, in *Isospin in Nuclear Physics*, edited by D. H. Wilkinson (Wiley, New York, 1969), Chap. 9.

[2]F. D. Becchetti, Jr. and G. W. Greenlees, Phys. Rev. 182, 1190 (1969).

[3]A. M. Lane, Phys. Rev. Lett. 8, 171 (1962); Nucl. Phys. 35, 676 (1962).

[4]J. D. Anderson and C. Wong, Phys. Rev. Lett. 7, 250 (1961).

[5]J. D. Carlson, C. D. Zafiratos, and D. A. Lind, Nucl.

Phys. A249, 29 (1975).
[6]S. D. Schery, D. A. Lind, H. W. Fielding, and C. D. Zafiratos, Nucl. Phys. A234, 109 (1974).
[7]R. K. Jolly, T. M. Amos, A. Galonsky, R. Hinrichs, and R. St. Onge, Phys. Rev. C 7, 1903 (1973).
[8]C. Wong, J. D. Anderson, J. W. McClure, B. A. Pohl, and J. J. Wesolowski, Phys. Rev. C 5, 158 (1972).
[9]C. H. Poppe, S. M. Grimes, J. D. Anderson, J. C. Davis, W. H. Dunlop, and C. Wong, Phys. Rev. Lett. 33, 856 (1974).
[10]S. M. Grimes, C. H. Poppe, J. D. Anderson, J. C. Davis, W. H. Dunlop, and C. Wong, Phys. Rev. C 11, 158 (1975).
[11]C. Wong, J. D. Anderson, J. C. Davis, and S. M. Grimes, Phys. Rev. C 7, 1895 (1973).
[12]D. M. Patterson, R. R Doering, and A. Galonsky, Nucl. Phys. A263, 261 (1976).
[13]P. S. Miller and G. T. Garvey, Nucl. Phys. A163, 65 (1971).
[14]G. W Hoffman, W. H. Dunlop, G. J. Igo, J. G. Kulleck, C. A. Whitten, Jr., and W. R. Coker, Phys. Lett. 40B, 453 (1972).
[15]P. D. Kunz, L. D. Rickertson, and G. W. Hoffman, Phys. Rev. C 9, 1659 (1974).
[16]G. T. Garvey and P. S. Miller, Phys. Lett. 28B, 243 (1968).
[17]A. I. Yavin, R. A. Hoffswell, L. H. Jones, and T. M. Noweir, Phys. Rev. Lett. 16, 1049 (1966).
[18]T. J. Woods, G. J. Igo, J. W. Sunier, J. W. Verba, C. A. Whitten, Jr., W. H. Dunlop, and G. W. Hoffman, Nucl. Instrum. Methods 94, 87 (1971).
[19]D. H. Fitzgerald, G. W. Greenlees, J. S. Lilley, J. M. Moss, and T. Woods, Phys. Rev. Lett. 34, 890 (1975).
[20]Electromagnetic Separation Group, Chemistry Division, A.E.R.E., Harwell.
[21]Supplied by Nuclear Enterprises Ltd., San Carlos, California.
[22]B. A. Pohl, J. D. Anderson, J. W. McClure, and C. Wong, Lawrence Livermore Laboratory Report No. UCRL-50653 (unpublished).
[23]N. Cue and P. Richard, Phys. Rev. 173, 1108 (1968).
[24]P. Richard, C. F. Moore, J. A. Becker, and J. D. Fox, Phys. Rev. 145, 971 (1966).
[25]P. D. Kunz, University of Colorado, private communication.
[26]G. W. Greenlees, W. Makofske, and G. J. Pyle, Phys. Rev. C 1, 1145 (1970).
[27]S. D. Schery, D. A. Lind, and Howard Wieman, Phys. Rev. C 14, 1800 (1976).
[28]C. J. Batty, E. Friedman, and G. W. Greenlees, Nucl. Phys. A127, 368 (1969).
[29]G. W. Hoffman and W. R. Coker, Phys. Rev. Lett. 29, 227 (1972).
[30]A. Bohr and B. Mottleson, *Nuclear Structure* (Benjamin, New York, 1969), Vol. I, p. 230.
[31]J. R. Beyster, M. Walt, and E. W. Salmi, Phys. Rev. 104, 1319 (1956); R. L. Becker, W. G. Guindon, and G. J. Smith, Nucl. Phys. 89, 154 (1966); S. Tanaka, Y. Tomita, Y. Yamanonti, and J. Ideno, in *Nuclear Structure Study with Neutrons*, edited by J. Erö and J. Szücs (Plenum, New York, 1974); M. Walt and J. R. Beyster, Phys. Rev. 98, 677 (1955); R. M. Wilenzick, K. K. Seth, P. R. Bevington, and H. W. Lewis, Nucl. Phys. 62, 511 (1965).
[32]D. G. Foster, Jr. and D. W. Glasgow, Phys. Rev. C 3, 576 (1971).
[33]Data compiled by M. H. MacGregor, D. E. Cullen, R. J. Howerton, and S. T. Perkins, UCRL Report No. UCRL 50400, 1976 (unpublished), Vol. 10, Rev. 1.
[34]B. Holmquist and T. Wiedling, Nucl. Phys. A188, 24 (1972).
[35]J. R. Huizenga and G. Igo, Nucl. Phys. 29, 462 (1962).
[36]A. Gilbert and A. G. W. Cameron, Can. J. Phys. 43, 1446 (1965).
[37]P. A. Moldauer, Rev. Mod. Phys. 36, 1079 (1964).